Enhanced Planar Channeling of MeV Protons through Thin Crystals

M. B. H. Breese, M. A. Rana, T. Osipowicz, and E. J. Teo

Physics Department, National University of Singapore, 10 Lower Kent Ridge Road, Singapore 119260

(Received 9 March 2004; published 3 September 2004)

At certain tilt alignments between a MeV proton beam and a planar channeling direction, a single interface lattice rotation within a crystal can result in a lower rate of dechanneling than at planar alignment in a perfect crystal. Such planar channeling enhancement arises when the beam passes through a layer thickness which is a half-multiple of the oscillation wavelength and then encounters a small interface rotation which is matched to the beam tilt angle. The beam is projected into the center of the phase space ellipse below the interface, resulting in certain trajectories undergoing a reduction in their transverse energy, in a manner analogous to stochastic cooling or atom laser cooling.

DOI: 10.1103/PhysRevLett.93.105505 PACS numbers: 61.85.+p, 07.78.+s, 41.85.–p, 61.72.–y

MeV ions that are channeled along a planar crystal direction are steered between the lattice walls, making periodic oscillations with depth [1]. Planar channeled protons lose energy at typically half the rate of non-channeled protons [2], and the proportion remaining channeled decreases exponentially with depth due to collisions with valence electrons [3]. The backscattered yield of channeled ions along off-normal directions in strained-layer superlattices is sensitive to the interaction of the planar oscillating beam with the periodic, rotated interfaces. Both catastrophic dechanneling [4,5] and resonance channeling [6,7] effects may occur, depending on the oscillation wavelength, λ, and the periodic layer thicknesses. Resonance channeling achieves the lowest rate of dechanneling through such a structure, but it is still higher than in a perfect crystal at planar alignment (hereafter called a "perfect crystal").

A phase space model of planar channeling [8] may be used to explain the relationship between beam tilt, interface depth, and oscillation wavelength for catastrophic dechanneling and resonance channeling [4–7]. The perpendicular angle of each ion is plotted versus its spatial position, x, with respect to the lattice plane walls. The channeled beam occupies an elliptical area bounded by $\pm x_c$ along the horizontal axis, this being the closest approach the ions make to the plane walls. The relationship

$$x_c = d_p/2 - 1.25a_{\mathrm{TF}}, \tag{1}$$

where d_p is the interplanar spacing and a_{TF} is the Thomas-Fermi screening length, was found to provide good agreement between theory and experiment [7]. Along the vertical axis, the distribution is bounded by the critical angle, equal to $\Psi_p = \pm 0.17°$ for 2 MeV protons along the Si{110} planes.

A lattice translation or rotation may be incorporated into a phase space model, respectively, as a horizontal or vertical displacement of the bounding ellipse below the fault plane, and they result in equivalent planar dechanneling effects [9]. Similar oscillations are produced in the simulated transmitted energy of channeled protons versus depth of a lattice rotation and a translation, with $\lambda/4$ difference in the depth dependence. Such oscillations were recently observed [10] for a 2 MeV proton beam focused to 60 nm along the silicon (011) planes ($d_p = 1.92$ Å), and scanned across the inclined plane of a stacking fault with a translation of 0.65 Å, equal to $d_p/3$. Even at fault depths corresponding to optimum transmission, the beam had a higher dechanneling rate than in a perfect crystal, with fewer high-energy protons transmitted.

This Letter describes conditions under which enhanced planar channeling is produced on passing through a single interface rotation, resulting in a dechanneling rate which is lower than in a perfect crystal. The Monte Carlo channeling code FLUX [11], which uses the Ziegler-Biersack-Littmark potential, and a binary collision model with an impact parameter dependent algorithm for energy loss were used to simulate channeled proton trajectories. Figure 1(a) shows the transmitted energy spectrum of 2 MeV protons, aligned with the {110} planes of a 10 μm thick silicon crystal, for which $\lambda = 210$ nm for small amplitude oscillations. The large low-energy

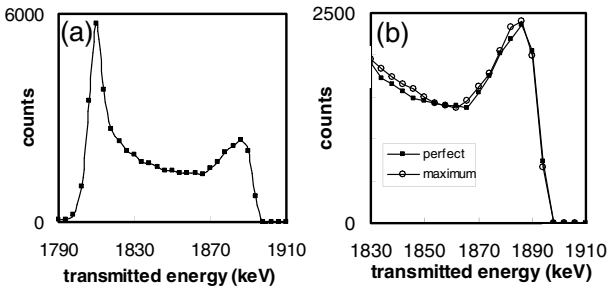

FIG. 1. (a),(b) Simulated energy spectra for 50 000 protons which are transmitted along the {110} planes of a perfect, 10 μm thick [100] Si crystal. Shown in (b) is the high-energy portion of the simulated energy spectrum at maximum enhancement.

peak contains those trajectories which are not channeled at the surface, or which have rapidly dechanneled. Those trajectories which are transmitted with energy >1870 keV have remained channeled through the entire thickness, confirmed by observing that their phase space locations are all confined within the bounding ellipse. Those in the central portion of the energy spectrum (1830–1870 keV) have dechanneled at some depth into the crystal.

Energy spectra for 2 MeV protons transmitted through the same 10 μm layer, now containing a single interface rotation of $\delta = 0.05°$ ($\sim 2\Psi_p/6$), were also simulated. Figure 2 shows the number of transmitted protons with energy >1870 keV, for this interface rotation at depths up to 3λ. For interface depths up to 2λ, the counts at $\phi = \pm 0.05°$ are greater than in a perfect crystal. This enhancement reaches a maximum for an interface depth of λ, hereafter called the condition for "maximum enhancement." Figure 1(b) also shows more counts in the central portion of the spectrum at maximum enhancement, indicating that the beam has undergone a lower rate of dechanneling throughout the remaining layer thickness beneath the interface.

Figure 3 demonstrates how planar enhancement is produced. The beam enters a perfect crystal as a horizontal line in phase space. The channeled beam component rotates clockwise within the ellipse, making one complete revolution each depth interval of λ, so at a depth of 210 nm in Fig. 3(a), many protons again lie on a horizontal line. Protons entering close to the lattice walls have a shorter oscillation wavelength owing to the nonharmonic nature of the planar potential, resulting in the spiral arms of the phase space distribution [12]. Figure 3(d) shows the phase space distribution of trajectories in Figs. 3(a)–3(c), plotted as a function of radial ordinate r, where

$$r^2 = \left(\frac{x}{x_c}\right)^2 + \left(\frac{\phi}{\psi_p}\right)^2. \quad (2)$$

Trajectories with smaller values of r have a lower probability dechanneling through the layer. Trajectories for which $r > 1$ may be considered as dechanneled, i.e., outside the bounding ellipse. The distribution of radial ordinates in Fig. 3(a) is quite uniform, except at small r which is depopulated with increasing depth due to multiple scattering, and large r which is depopulated by protons becoming dechanneled. Small changes to the bounding values of x_c and Ψ_p do not significantly alter the curves in Fig. 3(d).

In Fig. 3(b), most protons have rotated through slightly more than one complete revolution, giving a phase space distribution in which most trajectories occupy a tilted line. The central portion of the bounding ellipse is empty; hence there are few trajectories with $r < 0.2$ in Fig. 3(d). On encountering a lattice rotation of $\delta = \phi$ in Fig. 3(c) (maximum enhancement), those protons within the straight line portion become located close to the center of the new bounding ellipse, producing a number of trajectories with $r < 0.2$ which is only slightly less than for a perfect crystal. However, those trajectories within the upper spiral arm are now located closer to the new ellipse center, so there are more trajectories with $r \leq 0.6$,

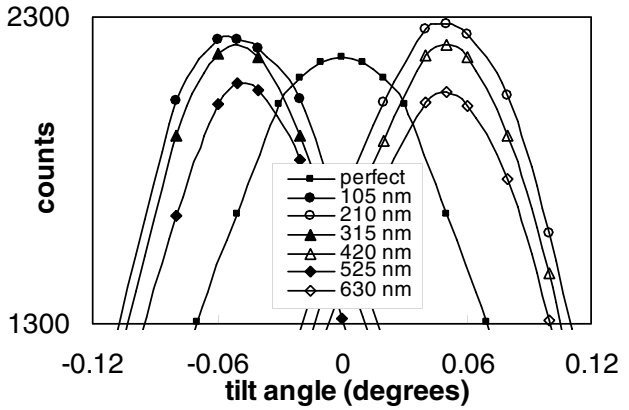

FIG. 2. Number of protons transmitted with energy >1870 keV versus tilt angle ϕ with respect to the {110} planes of the entrance layer, with an interface rotation at different depths corresponding to half-multiples of the oscillation wavelength. Also shown is the corresponding curve for a perfect crystal. 10 000 protons are simulated in each case.

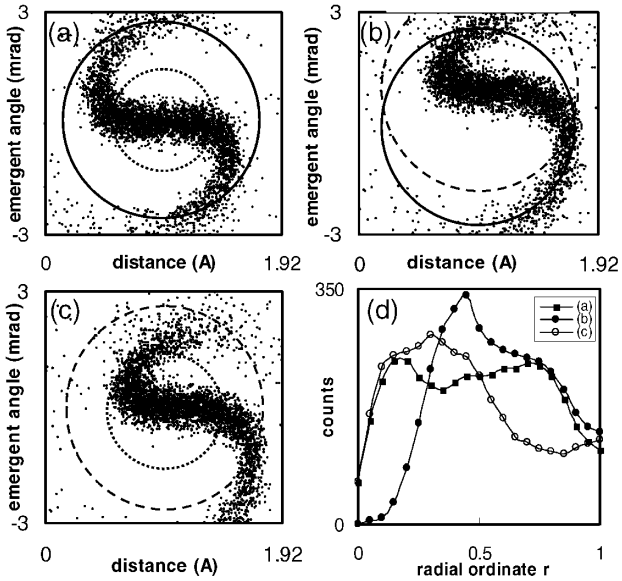

FIG. 3. Phase space plots along the {110} planes for 10 000 2 MeV protons at a depth of 210 nm. (a) Perfect crystal, $\phi = 0.00°$. (b) Perfect crystal, $\phi = 0.05°$. (c) Conditions for maximum enhancement, i.e., the same as (b) but with $\delta = 0.05°$ at a depth of λ. The bounding ellipse in the top 210 nm layer is shown as a solid line, and in the subsequent rotated layer as the dashed line. The ellipse containing those radial ordinates with $r < 0.6$ is shown as a dotted line. (d) Distribution of radial ordinates in each case.

within the dotted circle, than for a perfect crystal. These extra trajectories contribute additional counts to the portion of the planar enhanced spectrum shown in Fig. 1(b). The reduced rate of dechanneling associated with planar enhancement after the interface is further illustrated in Fig. 4. Apart from a narrow region of high dechanneling immediately after the interface in Fig. 4(b), there is a reduced dechanneling rate through the remaining layer thickness. This rises from ~90% of that in a perfect crystal immediately after the interface, to ~100% close to the exit face.

Planar enhancement has been experimentally observed in a $Si_{0.97}Ge_{0.03}$ epilayer with a thickness of 220 nm (measured by Rutherford backscattering spectrometry), grown on a [100] silicon substrate. Tetragonal lattice distortion results in an interface rotation angle of 0.06° ($\sim 2\Psi_p/6$) along the $(0\bar{1}1)$ planes close to the $[\bar{1}11]$ axis, located 54.7° away from the surface-normal direction (shown in the inset in Fig. 5). The (110) planes, which contain no interface rotation, can also be aligned with the beam by a small tilt away from the $[\bar{1}11]$ axis. Measurements along these two planar directions give a comparison of the transmitted energy spectra through the same layer thickness, for a perfect layer and a rotated layer along which planar enhancement may occur.

The path length through the epilayer close to the $[\bar{1}11]$ axis is ~380 nm. For planar enhancement the epilayer thickness has to be a half-multiple of λ, where $\lambda =$ 210 nm in the above simulations, compared with a measured value of 185 nm at $\phi = 0.05°$ [10]. The wavelength varies as $\lambda \propto \sqrt{E}$ [13]; hence a change of 300 keV in the beam energy of 2 MeV changes the wavelength by 13–15 nm. This results in enhancement disappearing in simulations for a given interface depth, since the beam can no longer be projected into the center of the ellipse beneath the interface. Transmitted energy spectra were recorded for a range of proton energies above and below 2 MeV to search for the correct wavelength conditions to produce planar enhancement through a layer thickness of 2λ.

The sample was mechanically thinned and polished to a thickness of 10 μm and mounted with a charged particle detector (resolution of 15 keV) on the beam axis immediately behind it which recorded all transmitted protons. Figure 5 shows the best channeled transmitted energy spectra along the straight (110) planes, and the rotated $(0\bar{1}1)$ planes for beam energies of 1.9 and 2.2 MeV. At 1.9 MeV, planar enhancement results in the $(0\bar{1}1)$ spectrum having more counts outside the low-energy peak than the (110) spectrum, whereas at 2.2 MeV (and all other recorded energies) the opposite is true. At 1.9 MeV the effect of planar enhancement is more pronounced along the central portion of the spectrum, with only a small increase observed in the high-energy peak. This is due to the layer thickness of ~17 μm in the measurements compared with 10 μm in the simulations, resulting in fewer protons remaining channeled throughout the layer.

Enhanced planar channeling occurs when the beam tilt is matched to a small lattice rotation of $\sim 2\Psi_p/6$ at depths equal to half-multiples of λ. Enhancement disappears in simulations for interface depths greater than 2λ because the spiral arms of the phase space distribution become too extended to be captured by a lattice rotation. Enhancement does not occur for much smaller or larger rotations because the spiral arms of the distribution are, respectively, not sufficiently folded back or too extended to be adequately captured by a lattice rotation. Enhancement has also been observed in simulations of a bilayer containing an interface translation of $2x_c/6$, i.e., a shift along the horizontal axis of the bounding ellipse by a similar

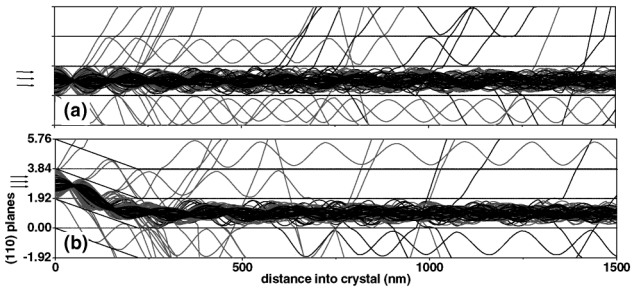

FIG. 4. Trajectories of 100 2 MeV protons along the {110} planes, for (a) a perfect crystal and (b) maximum enhancement. Those trajectories which remain channeled to a depth of 10 μm are plotted in black. Dechanneled trajectories are shown in gray, apart from those which have dechanneled between depths of 500 to 1500 nm which are shown in thick black lines. There are 13 trajectories which become dechanneled between these depths in (a) compared to 9 in (b).

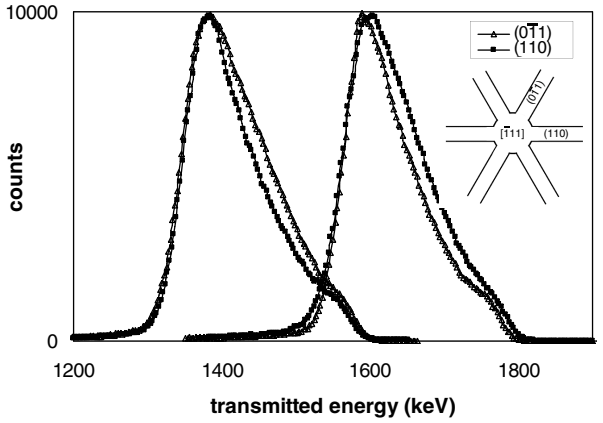

FIG. 5. Measured energy spectra for 1.9 MeV (to the left) and 2.2 MeV protons (to the right) transmitted through a $Si_{0.97}Ge_{0.03}/Si$ bilayer close to the $[\bar{1}11]$ axis. The (110) planes correspond to a perfect layer, and the $(0\bar{1}1)$ planes contain an interface rotation of 0.06°. The spectra are normalized to the same height of the low-energy peak to emphasize the different behavior observed in the high-energy portion of the spectra.

fraction. However, experimental observation of such enhancement at stacking faults is not currently possible since it would require a beam spot of less than 10 nm.

This Letter has demonstrated conditions which produce better planar channeling than in a perfect crystal, a result not previously predicted using classical channeling theory owing to the specific combination of beam/crystal parameters required. Certain proton trajectories are corrected, or "cooled," by reducing their angle and hence transverse energy at a specific depth, in a manner analogous to other cooling mechanisms. In all cases, the phase space ordinates of selected particles are compressed by shifting them towards the center of the distribution. For example, stochastic cooling of antiprotons [14] uses feedback correction to adjust particle orbits around a radio-frequency debuncher to reduce the particle beam energy spread, and atom laser cooling [15] uses a feedback-controlled laser wavelength and power to minimize residual thermal energy.

E. J. T. acknowledges financial support from the Singapore Millennium Foundation.

[1] D. Gemmell, Rev. Mod. Phys. **46**, 129 (1974).
[2] B. R. Appleton, C. Erginsoy, and W. M. Gibson, Phys. Rev. **161**, 330 (1967).
[3] L. C. Feldman and B. R. Appleton, Phys. Rev. B **8**, 935 (1973).
[4] W. K. Chu, J. A. Ellison, S. T. Picraux, R. M. Biefeld, and G. C. Osbourn, Phys. Rev. Lett. **52**, 125 (1984).
[5] S. T. Picraux, W. R. Allen, R. M. Biefeld, J. A. Ellison, and W. K. Chu, Phys. Rev. Lett. **54**, 2355 (1985).
[6] J. A. Ellison, S. T. Picraux, W. R. Allen, and W. K. Chu, Phys. Rev. B **37**, 7290 (1988).
[7] W. R. Allen, W. K. Chu, S. T. Picraux, R. M. Biefeld, and J. A. Ellison, Phys. Rev. B **39**, 3954 (1989).
[8] J. A. Ellison, Nucl. Phys. **B206**, 205 (1982).
[9] M. B. H. Breese and P. J. M. Smulders, Phys. Rev. Lett. **81**, 5157 (1998).
[10] M. B. H. Breese, E. J. Teo, M. A. Rana, L. Huang, J. A. van Kan, F. Watt and P. J. C. King, Phys. Rev. Lett. **92**, 045503 (2004).
[11] P. J. M. Smulders and D. O. Boerma, Nucl. Instrum. Methods Phys. Res., Sect. B **29**, 471 (1987).
[12] M. B. H. Breese and P. J. M. Smulders, Nucl. Instrum. Methods Phys. Res., Sect. B **145**, 346 (1998).
[13] D. van Vliet, Radiat. Eff. **10**, 137 (1971).
[14] D. Mohl, G. Petrucci, L. Thorndahl and S. van der Meer, Phys. Rep. **58**, 76 (1980).
[15] S. Chu, Science **253**, 861 (1991).